Reversible Switching of the Interparticle Distance in DNA-Templated Gold Nanoparticle Dimers

Laurent Lermusiaux,[†] Alexandra Sereda,[†] Benjamin Portier,[†] Eric Larquet,[‡] and Sébastien Bidault[†,*]

[†]Institut Langevin, ESPCI ParisTech, CNRS UMR 7587, INSERM U979, 1, rue Jussieu, 75005 Paris, France and [‡]Laboratoire d'Enzymologie et Biochimie Structurales, CNRS UPR 3082, avenue de la Terrasse, 91198 Gif-sur-Yvette, France

ABSTRACT We produce gold nanoparticle dimers with a surface-to-surface distance that varies reversibly by a factor of 3 when hybridizing or removing a single target DNA strand. The dimers are built on one DNA template that features a stem-loop enabling the interparticle distance change. Using electrophoresis, we reach 90% sample purities and demonstrate that this chemical process is reversible in solution at room temperature for a low molar excess of the target DNA strand. The kinetics of the reaction is asymmetric due to steric hindrance in the stem-loop opening process. Furthermore, a statistical analysis of cryo-electron microscopy measurements allows us to provide the first quantitative analysis of distance changes in chemically switchable nanoparticle assemblies.

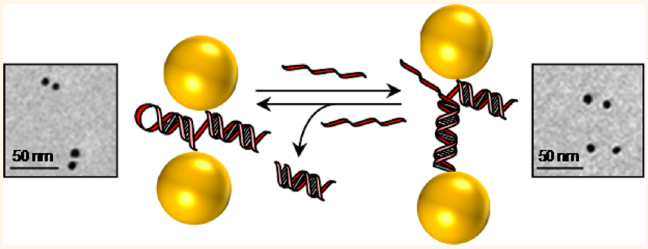

KEYWORDS: dynamic nanostructures · DNA self-assembly · gold nanoparticles · cryo-electron microscopy · electrophoresis

Building nanostructures whose shape and physical properties are sensitive to their local environment is an essential step toward novel therapeutic[1−4] and sensing[5−9] strategies. Thanks to its structural plasticity and the reversibility of its interactions, DNA is a great candidate to build nanoobjects that are dynamic, reconfigurable, and responsive.[10] Moreover, the ability to select and chemically modify each base of a DNA sequence allows structural control down to a base-to-base distance of one-third of a nanometer[11−14] and unparalleled conjugation possibilities to inorganic nanoparticles.[15−17] An attractive way to translate the conformational changes of DNA molecules into macroscopically measurable signals is to functionalize them with optically active entities. In particular, electromagnetically coupled chromophore pairs have led to the development of molecular beacons[5] and have allowed the study of dynamic 2D and 3D DNA nanostructures using Förster resonant energy transfer (FRET).[18−22] Because of their resonant optical responses, photostability,[23] and photothermal properties,[24,25] gold nanoparticles (AuNPs) are an interesting alternative to dye molecules. While dynamic AuNP−DNA conjugates have already been demonstrated in the literature,[8,26−29] substrate induced aggregation, sample inhomogeneity and particle nonsphericity have hindered a quantitative analysis of their conformational changes. In this study, we produce the simplest dynamic AuNP−DNA architecture—particle dimers linked by a single stem-loop containing DNA sequence—and demonstrate that a precise measurement of the interparticle distance change, when opening the loop, is possible using cryo-electron microscopy (cryo-EM). Furthermore, a single-stranded overhang renders the conformational change reversible at room temperature, as observed in electrophoresis. We demonstrate that the kinetics of the stem-loop conformation change in AuNP dimers is asymmetric with a favored closing step.

RESULTS AND DISCUSSION

We produce dimers of 8 nm diameter AuNPs in two conformations using a single dynamic DNA scaffold as described in Scheme 1. One half of the DNA template (sequence **S**) contains a 10 bp stem-loop which opens when hybridizing a **T** single-strand.

* Address correspondence to sebastien.bidault@espci.fr.

Received for review October 4, 2012 and accepted November 2, 2012.

Published online November 02, 2012
10.1021/nn304599d

The 100 bases-long **S** sequence can hybridize to a complementary **C** DNA molecule over 50 bp. As discussed in previous reports,[26,30−36] we use electrophoresis to separate 8 nm AuNPs linked to a single trithiolated **S**, **C** or **S**+**T** DNA molecule, yielding structures **1**, **2**, and **3** of Scheme 1. This technique is compatible with particles as large as 40 nm in diameter if the length of the grafted DNA strand increases the hydrodynamic volume of the conjugate sufficiently for efficient separation.[14,35] For this reason, sequence **C** is hybridized over 15 bp to a 100 base-long lengthening single-strand **L** prior to electrophoresis to optimize the purification of monoconjugated AuNPs.[26,35] Closed (**4**) and open (**5**) dimers are obtained by hybridizing structures **1**+**2** and **2**+**3**, respectively, followed by electrophoretic purification. Sequences **S** and **C** feature trithiolated modifications at their 5′ and 3′ ends, respectively, in order to minimize the interparticle distance in **4** with a 50 bp double-strand perpendicular to the dimer axis.[35,36] A 30 bases-long single strand overhang in **T** of **S**+**T** is designed to allow the reversible shift between **4** and **5** by adding the complementary **T**′ DNA molecule.[18] DNA functionalizations and subsequent hybridizations are performed in the presence of charge screening cations (Na^+) to compensate repulsive interactions between negatively charged DNA molecules and AuNPs.[30−37] Furthermore, to minimize these electrostatic interactions during the dimer formation, and to increase the dimer suspension stability, DNA-functionalized AuNPs are passivated by an excess of methyl-terminated thiolated ethylene glycol oligomers prior to electrophoretic purification.[35,37]

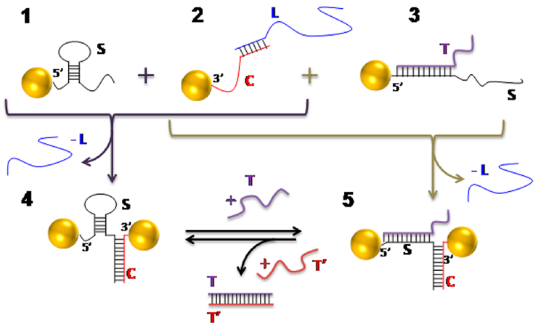

Scheme 1. Dynamic dimer synthesis.

The modification of hydrodynamic volume and surface charges when opening or closing the loop is directly visible during electrophoretic purification for both DNA-conjugated AuNPs and hybridized dimers as demonstrated on Figure 1. Figure 1a shows the efficient purification of structures **1**, **2**, and **3** after electrophoresis in a 2.5% weight-to-weight agarose gel. The significantly different electrophoretic mobilities of **1** and **3** demonstrate that all monoconjugated AuNPs feature either closed or open stem-loops. Structures **4** and **5** also feature different mobilities as shown in Figure 1b when purifying dimers from remaining single AuNPs and subpopulations of higher assemblies after hybridization. The position difference in the agarose gel is more visible in cross sections along the migration path (see Figure 1c). Each band on the gel image is materialized as a peak whose position is related to the

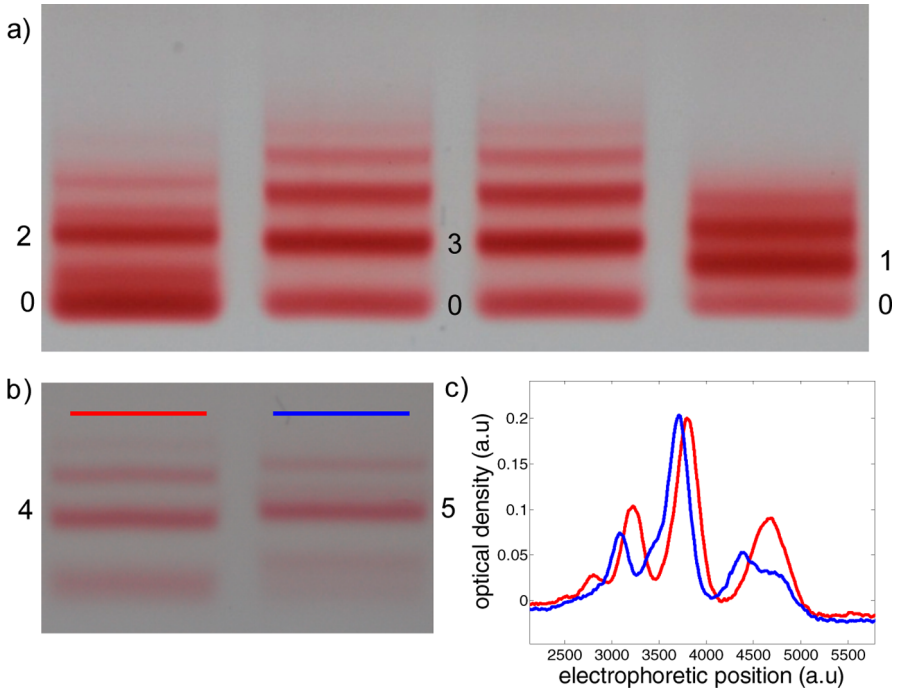

Figure 1. (a) Electrophoretic purification of structures 1, 2, and 3. Band 0 corresponds to unconjugated 8 nm AuNPs and higher bands to multiconjugated particles. (b) Electrophoretic purification of closed (4) and open (5) dimers. (c) Cross sections of the two columns of panel b along the migration axis.

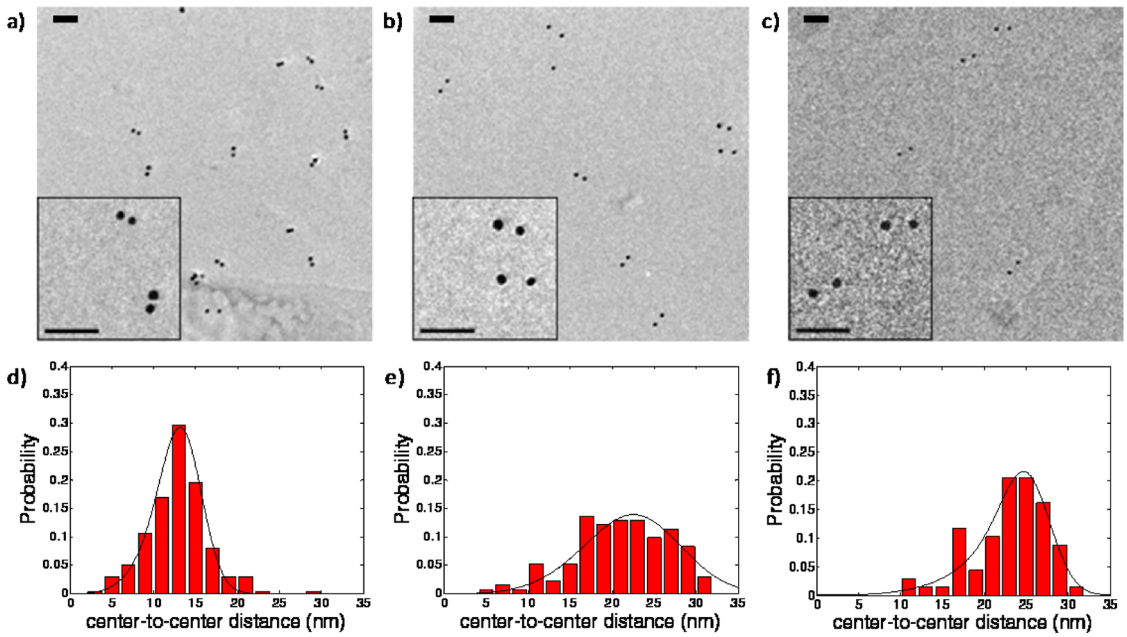

Figure 2. Cryo-EM images of closed (4,a) and open (5,b) 8 nm AuNP dimers at 50 mM NaCl (scale bars = 50 nm, insets correspond to close-ups). (c) Cryo-EM image of 5 at 1 mM NaCl. (d) Center-to-center distance distributions of 4. (e,f) Center-to-center distance distributions of 5 for two NaCl concentrations: 50 mM (e) and 1 mM (f). Solid black lines correspond to a Gaussian fit taking into account the orientation of the dimers with respect to the electron beam.

size and charge of the nanostructure, the fastest objects being shifted to the right of the plot and the highest peaks corresponding to dimers. The peak related to **4** (closed dimer) on the red plot is thus located at the right of the dimer peak on the blue plot (**5**), demonstrating that the conformational change of dynamic AuNP dimers is directly visible in electrophoresis.

To obtain a quantitative estimation of interparticle spacings in DNA templated dimers, we image them in cryo-electron microscopy. This technique allows the characterization of nanoparticle groupings as they are in solution without the influence of drying effects or substrate interactions.[35,38,39] Typical cryo-EM images are shown in Figure 2a,b for **4** and **5**, respectively, measured in a 50 mM NaCl solution. This salt concentration is lower than for the preparation of samples **1** through **5** (80 mM NaCl) to minimize particle aggregation that would impede cryo-EM image analysis. Furthermore, while cations are necessary for the thermodynamic stability of the short DNA loop in **4**, **5** can be studied at low salt concentrations (1 mM) as shown on Figure 2c. Estimated purities for closed and open dimers are 92% and 88%, respectively. A statistical analysis of center-to-center interparticle distances is performed on 432 dimers (in 80 cryo-EM images) by fitting the particles with spheres. Distributions for **4** and **5** are given in Figure 2d−f. Figure 2 thus clearly demonstrates the significant shape modification induced by hybridizing or removing a single DNA strand in AuNP dimers.

To obtain the surface-to-surface distance change between **4** and **5**, we need to take into account the diameter distribution of AuNPs and the angle between the electron beam and the sample. Indeed, the vitreous water film formed on the carbon grid being several tens of nanometers thick,[38,39] a cryo-EM image corresponds to the two-dimensional projection of the three-dimensional sample as discussed in a previous report.[35] The solid black lines in Figure 2 panels d−f correspond to Gaussian distributions of the surface-to-surface interparticle distances convoluted by the diameter distribution and projected in the plane perpendicular to the electron beam (see Methods for details). These fits indicate surface-to-surface distances of 5.5 ± 1.2 nm for the closed dimer (**4**) and 15.5 ± 2.6 nm for the open dimer (**5**) at 50 mM NaCl. It is thus possible to design nanoparticle assemblies in which the interparticle distance varies by nearly a factor of 3 when adding a single target molecule.

Furthermore, we observe a clear increase of the distance standard deviation for open dimers. The rigidity of DNA templated AuNP dimers strongly depends on repulsive electrostatic interactions[8,35,40] which are significantly reduced when increasing the interparticle distance by a factor of 3. In practice, closed dimers (**4**) seem stretched by electrostatic interactions since the DNA linker is approximately 4 nm long (width of 2 DNA helices) while the obtained distance in open form (**5**) is significantly lower than the size of the DNA template (17 nm for the length of the **S**+**T** 50 bp spacer and 2 nm for the width of the **S**+**C** linker). However, when studying sample **5** at low ionic strength (1 mM NaCl) in Figure 2c,f, we observe an increase of the interparticle distance (17.5 nm) and a reduction of the standard deviation (±1.3 nm). In this case, the obtained distance is similar to the length of the DNA template,

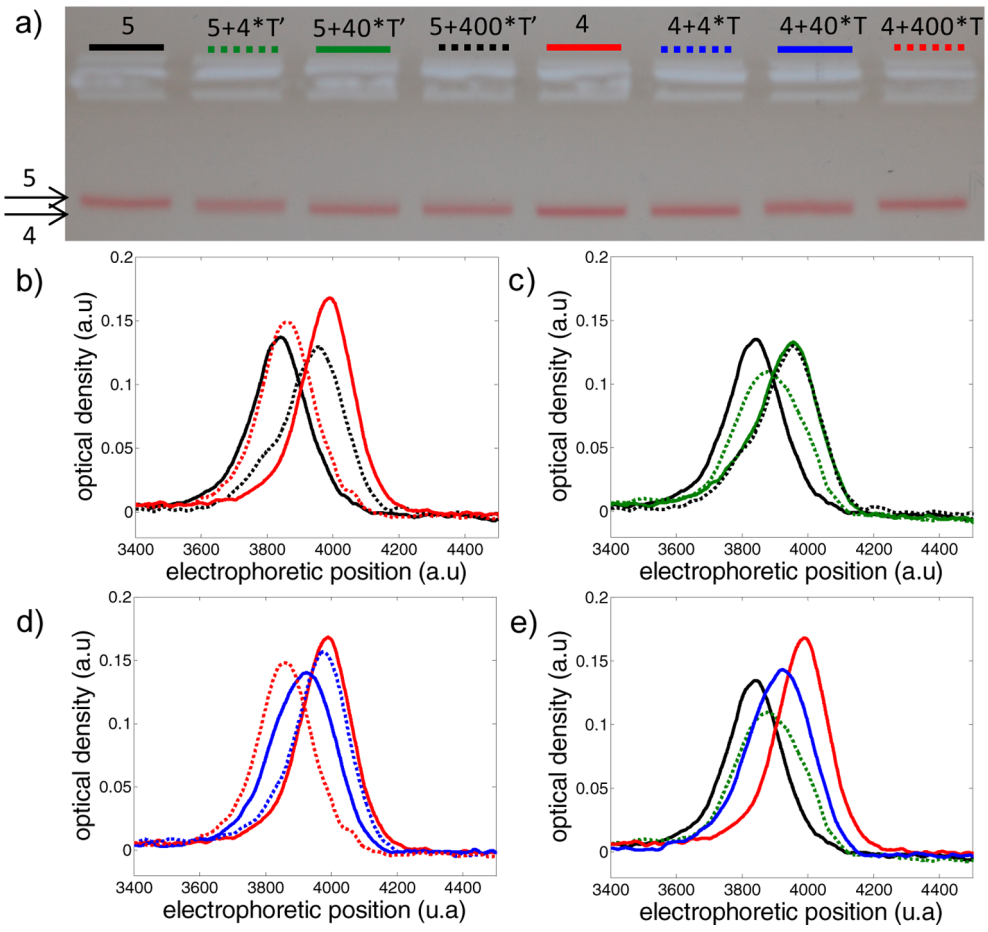

Figure 3. (a) Electrophoretic analysis of dynamic 8 nm dimers after incubation with different excesses of T and T′. Side arrows indicate the position of reference samples of 4 and 5. (b–e) Cross sections along the migration axis of the 8 columns of panel a.

indicating stretched dimers. Increased dimer rigidity due to stronger repulsive electrostatic interactions at low ionic strengths thus leads to a narrower distribution of interparticle distances in sample **5**.

Since electrophoresis can indicate the shape of the dynamic dimers, it can be used to easily test the efficiency and reversibility of the DNA loop opening. Plasmon resonance spectroscopy is not applicable in this case as the interparticle distances in **4** and **5** are larger than the particle radii and would lead to negligible electromagnetic coupling of the particle resonances.[8,35,37] In practice, the dimer opening and closing reactions are both thermodynamically allowed with an overall gain of 40 and 30 base pairing events when going from **4** to **5** and *vice versa* (neglecting entropy). After incubating **4** and **5** with varying excess concentrations of **T** and **T′** (from 4 to 400) for 30 min at room temperature in 80 mM NaCl, we characterize the final nanostructures in electrophoresis. Single bands are observed on Figure 3a for all samples, demonstrating that DNA loop opening does not alter the synthesized dimers. Furthermore, the electrophoretic mobility of the obtained samples is included between reference open and closed dimers indicated by the side arrows (columns 1 and 5 corresponding to samples **5** and **4**, respectively). Figure 3b provides the vertical cross sections for **5** (black solid line), **5** + **400*T′** (dashed black line), **4** (red solid line), and **4** + **400*T** (red dashed line). The peaks corresponding to **4** and **5** are nearly overlaid with **5** + **400*T′** and **4** + **400*T**, respectively, indicating that the reaction is complete and reversible in both directions. The reversible opening of the DNA stem-loop was performed successfully 3 times in a row in different experimental conditions, further confirming the robustness of the process (see SI).

By reducing the excess of target DNA strands, we observe that closing the loop is more favorable than opening it. Figure 3c shows the relative electrophoretic mobilities of samples **5**, **5** + **4*T′** (green dashed line), **5** + **40*T′** (green solid line), and **5** + **400*T′**. While the reaction is complete for **5** + **40*T′**, **5** + **4*T′** features a wide peak consistent with a weighted sum of the peaks corresponding to **4** and **5**. This result indicates a mixed population of open and closed dimers. To further verify this point, we mix equal amounts of **4** and **5** before electrophoretic analysis (data not shown). In that case, we also observe one band, even for long gel running times, suggesting that the electrophoretic mobility

difference between open and closed dimers is beyond the separation resolution of electrophoresis in these experimental conditions.

Identical reaction conditions for closed dimers provide significantly different results in Figure 3d. Indeed, the **4** + **4*T** sample (blue dashed line) is nearly overlaid with the reference **4** sample while the **4** + **40*T** (blue solid line) sample is a combination of open and closed dimers. The asymmetry in reactivity is clearer in Figure 3e as samples **5** + **4*T′** and **4** + **40*T** correspond to similar electrophoretic mobilities even though a 10 times larger excess of the target DNA strand is used to open the loop. This phenomenon is probably due to increased steric hindrance in closed dimers when interacting with **T**, leading to higher activation energies.

CONCLUSION

In summary, we produced gold nanoparticle dimers linked by a single dynamic DNA template. The interparticle distance varies reversibly by a factor of 3 in mild experimental conditions and for a low molar excess of the target DNA strand when opening the stem-loop. Combined with the optical properties of gold nanoparticles at their plasmon resonance, the 10 nm interparticle distance change provides numerous opportunities for the design of biochemical sensors, down to the single molecule level, and chemically switchable photothermal agents. In particular, our fabrication procedure is compatible with AuNPs up to 40 nm diameters that provide significant optical absorption and scattering cross sections.[14,35] Furthermore, the design of the DNA template is flexible as the single-stranded overhang, necessary for the kinetically favored dimer closing step, is independent of the rest of the scaffold and can include an aptamer sequence[41] to be sensitive to a broad range of (bio)chemical analytes.

METHODS

General. Citrate coated 8 nm diameter gold nanoparticles (AuNPs) were purchased from BBInternational (UK). Bis-(*p*-sulfonatophenyl)phenylphosphine (BSPP) was obtained from Strem Chemicals Europe (France). Thiolated, methyl terminated ethylene glycol oligomers ($n = 6$) were purchased from Polypure (Norway). Solvants and other buffer solutions were obtained from Sigma-Aldrich (USA). PAGE-purified trithiolated DNA sequences were purchased from Fidelity Systems, Inc. (USA). PAGE-purified unmodified DNA sequences were obtained from Integrated DNA Technologies Europe (Belgium). All chemicals were used as received without further purification. The different DNA sequences, designed to minimize nonspecific interactions, are the following:

S: 5′-trithiol-GGCTTACATGAGGAGCTAGGATACTTCCTGT-GAAGGTAACTAGCTCCTC TGCACGAAACCTGG ACACCCCTAAG-CAACTCCGTATCAGATGGGAACAGCA-3′

C: 5′-TGCTGTTCCCATCTGATACGGAGTTGCTTAGGGGTGTC-CAGGTTTCGTGC-trithiol-3′

L: 5′-ATCCTGACATCGGCATTTTTTTTTTTTTTTTTTTTTTTTTT-TTTTTTTTTTTTTTT TTTTTTTTTTTTTTTT TTTTTTTGTGCTGTTCC-CATCTG-3′

T: 5′-TACGATAGTGGTATGATCGCTAGATCCGCAAGAGGAGC-TAGTTACCTTCACAG GAAGTATCCTAGCTCCT CATGTAAGCC-3′

Synthesis of Gold Nanoparticle/DNA Conjugates. AuNPs are coated with BSPP following published procedures.[30−36] The final AuNP concentration is of the order of 1 pmol/μL.

To prepare structures **2** and **3**, **C**+**L** and **S**+**T** thiolated DNA molecules are hybridized by mixing 16 pmol of **C** (respectively 12 pmol of **S**) with a 2-fold excess of **L** (respectively **T**) in a 125 mM NaCl solution with a final 8 μL volume. The solution is heated at 80 °C and left to cool to room temperature overnight. A 3 μL of aliquot of 8 nm AuNPs solution are added to the **C**+**L** and **S**+**T** solutions as well as a 10 μL solution of **S** (12 pmol in 125 mM NaCl) for structure **1**. All solutions are left to incubate overnight at room temperature. The final volume is 12.5 μL with 80 mM NaCl and 10 mM BSPP final concentrations. The added BSPP is used as a reducing agent to minimize oxidation of the thiol moieties.[35] Surface passivation of the gold particle surface is obtained by incubating for 30 min a 50 000 excess of thiolated ethylene glycol oligomers[35,37] prior to electrophoretic purification in 2.5% agarose gels (Ficoll 400, 20% solution as loading buffer and 0.5x Tris-Borate-EDTA as running buffer). The gels are run at 8 V/cm for about 1 h before obtaining the results shown on Figure 1a of the manuscript. The extraction procedure is done following published protocols,[36] and the sample is concentrated by centrifugation.

Synthesis, Purification, And Reversible Switching of Particle Dimers. Stoichiometric amounts of **2** and **1** or **3** (~100 nM solutions) are mixed in 80 mM NaCl before being heated up to 50 °C and left to cool overnight to yield **4** and **5** (final volume ~10−15 μL). The samples are then electrophoretically purified in 2% agarose gels (Figure 1b). The bands are cut from the gel and the groupings are eluted in running buffer. Suspensions of **4** and **5** are stored in running buffer at 4 °C before Cryo-EM measurements or dimer opening/closing experiments.

The dimer switching experiments analyzed in Figure 3 are performed as follows: dimer suspensions of **4** and **5** are mixed, respectively, with varying excesses (4, 40, or 400) of **T** and **T′** in 80 mM NaCl for 30 min (~10−15 μL final volume). The samples are then analyzed in a 2% agarose electrophoresis gel. Protocols for the three-time consecutive dimer switching experiment are given in the Supporting Information.

Cryo-EM Characterization. The samples are observed with transmission electron microscopy in a cryogenic environment. The experimental procedures of the Cryo-EM sample preparation are described elsewhere.[35] The particle diameter distribution is estimated by fitting the AuNPs with a circle on the cryo-EM images. The distribution (based on 841 single particles) is plotted in Figure S2 of the Supporting Information along with a Gaussian fit corresponding to an 8.5 nm average diameter and a ±0.6 nm standard deviation. The measured distributions of interparticle distances given in Figure 2 are obtained by analyzing the cryo-EM images and estimating the center-to-center distance between two circles that best fit the AuNPs. The distributions on Figures 2d, 2e, and 2f were estimated on 236, 132, and 64 dimers, respectively. The widths of the distributions arise from three contributions: distribution of particle diameters, distribution of interparticle gaps, and projection of the dimer axis on the plane perpendicular to the electron beam.[35] The distributions of interparticle gaps, s, need to be estimated to understand the geometries of the DNA linkers. If l is the interparticle distance (sum of s and the diameter of the AuNPs) and $\tilde{l}$ the measured projected distance, then the distribution of $\tilde{l}$ can be expressed as

$$D_{\tilde{l}}(\tilde{l}) = \int_{\tilde{l}}^{+\infty} D_l(l)\, D_\theta(l,\tilde{l})\, \frac{\tilde{l}}{l}\, \frac{1}{\sqrt{l^2 - \tilde{l}^2}}\, dl$$

$D_l(l)$ is the convolution of the unknown gap distribution with the diameter distribution given in Supporting Information Figure S2

and readily fitted by Gaussian distributions. $D_\theta(l,\tilde{l})$ is the distribution of the angle θ between the dimer axis and the electron beam. The mathematical form $D_\theta(l,\tilde{l})$ that better reflects the geometry of the cryo-EM sample and allows us to fit experimental distributions of $\tilde{l}$ is $D_\theta(l,\tilde{l}) = (2/\pi)(\tilde{l}/l)^2$ as discussed in the literature.[35]

Conflict of Interest: The authors declare no competing financial interest.

Acknowledgment. The Authors acknowledge the *PICT-IBiSA* Imaging Facility of the Institut Curie—Orsay. This work is supported by Agence Nationale de le Recherche *via* project ANR-11-JS10-0002, CNRS program "Interface Physique Chimie Biologie: Soutien à la prise de risque" and by the Region Ile-de-France in the framework of C'Nano IdF. C'Nano IdF is the nanoscience competence center of Paris Region, supported by CNRS, CEA, MESR, and Region Ile-de-France. L.L. acknowledges a predoctoral grant from Fondation Pierre-Gilles de Gennes pour la Recherche.

Supporting Information Available: Three-time consecutive dimer switching experiments and diameter distribution of gold nanoparticles. This material is available free of charge *via* the Internet at http://pubs.acs.org.

REFERENCES AND NOTES

1. Lee, E. S.; Kim, D.; Youn, Y. S.; Oh, K. T.; Bae, Y. H. A Virus-Mimetic Nanogel Vehicle. *Angew. Chem., Int. Ed.* **2008**, *47*, 2418–2421.
2. Esser-Kahn, A. P.; Sottos, N. R.; White, S. R.; Moore, J. S. Programmable Microcapsules from Self-Immolative Polymers. *J. Am. Chem. Soc.* **2010**, *132*, 10266–10268.
3. Douglas, S. M.; Bachelet, I.; Church, G. M. A Logic-Gated Nanorobot for Targeted Transport of Molecular Payloads. *Science* **2012**, *335*, 831–834.
4. Zhao, Y. X.; Shaw, A.; Zeng, X. G.; Benson, E.; Nystrom, A. M.; Hogberg, B. DNA Origami Delivery System for Cancer Therapy with Tunable Release Properties. *ACS Nano* **2012**, 10.1021/nn3022662.
5. Tyagi, S.; Kramer, F. R. Molecular Beacons: Probes that Fluoresce upon Hybridization. *Nat. Biotechnol.* **1996**, *14*, 303–308.
6. Lee, J.; Govorov, A. O.; Kotov, N. A. Nanoparticle Assemblies with Molecular Springs: A Nanoscale Thermometer. *Angew. Chem., Int. Ed.* **2005**, *44*, 7439–7442.
7. Lee, J.; Hernandez, P.; Lee, J.; Govorov, A. O.; Kotov, N. A. Exciton-Plasmon Interactions in Molecular Spring Assemblies of Nanowires and Wavelength-Based Protein Detection. *Nat. Mater.* **2007**, *6*, 291–295.
8. Chen, J. I. L.; Chen, Y.; Ginger, D. S. Plasmonic Nanoparticle Dimers for Optical Sensing of DNA in Complex Media. *J. Am. Chem. Soc.* **2010**, *132*, 9600–9601.
9. Wang, L. B.; Xu, L. G.; Kuang, H.; Xu, C. L.; Kotov, N. A. Dynamic Nanoparticle Assemblies. *Acc. Chem. Res.* **2012**, 10.1021/ar200305f.
10. Seeman, N. C. DNA in a Material World. *Nature* **2003**, *421*, 427–431.
11. Heilemann, M.; Tinnefeld, P.; Mosteiro, G. S.; Garcia-Parajo, M.; Van Hulst, N. F.; Sauer, M. Multistep Energy Transfer in Single Molecular Photonic Wires. *J. Am. Chem. Soc.* **2004**, *126*, 6514–6515.
12. Acuna, G. P.; Bucher, M.; Stein, I. H.; Steinhauer, C.; Kuzyk, A.; Holzmeister, P.; Schreiber, R.; Moroz, A.; Stefani, F. D.; Liedl, T.; *et al*. Distance Dependence of Single-Fluorophore Quenching by Gold Nanoparticles Studied on DNA Origami. *ACS Nano* **2012**, *6*, 3189–3195.
13. Busson, M. P.; Rolly, B.; Stout, B.; Bonod, N.; Bidault, S. Accelerated Single Photon Emission from Dye Molecule-Driven Nanoantennas Assembled on DNA. *Nat. Commun.* **2012**, *3*, 962.
14. Busson, M. P.; Rolly, B.; Stout, B.; Bonod, N.; Wenger, J.; Bidault, S. Photonic Engineering of Hybrid Metal—Organic Chromophores. *Angew. Chem., Int. Ed.* **2012**, *51*, 11083–11087.
15. Fu, A. H.; Micheel, C. M.; Cha, J.; Chang, H.; Yang, H.; Alivisatos, A. P. Discrete Nanostructures of Quantum Dots/Au with DNA. *J. Am. Chem. Soc.* **2004**, *126*, 10832–10833.
16. Pal, S.; Deng, Z. T.; Ding, B. Q.; Yan, H.; Liu, Y. DNA-Origami-Directed Self-Assembly of Discrete Silver-Nanoparticle Architectures. *Angew. Chem., Int. Ed.* **2010**, *49*, 2700–2704.
17. Yan, W. J.; Xu, L. G.; Ma, W.; Xu, C. L.; Kuang, H.; Wang, L. B.; Kotov, N. A. Self-Assembly of Chiral Nanoparticle Pyramids with Strong R/S Optical Activity. *J. Am. Chem. Soc.* **2012**, *134*, 15114–15121.
18. Yurke, B.; Turberfield, A. J.; Mills, A. P.; Simmel, F. C.; Neumann, J. L. A DNA-Fuelled Molecular Machine Made of DNA. *Nature* **2000**, *406*, 605–608.
19. Chen, Y.; Mao, C. D. Putting a Brake on an Autonomous DNA Nanomotor. *J. Am. Chem. Soc.* **2004**, *126*, 8626–8627.
20. Aldaye, F. A.; Sleiman, H. F. Modular Access to Structurally Switchable 3D discrete DNA Assemblies. *J. Am. Chem. Soc.* **2007**, *129*, 13376–13377.
21. Goodman, R. P.; Heilemann, M.; Doose, S.; Erben, C. M.; Kapanidis, A. N.; Turberfield, A. J. Reconfigurable, Braced, Three-Dimensional DNA Nanostructures. *Nat. Nanotechnol.* **2008**, *3*, 93–96.
22. Andersen, E. S.; Dong, M.; Nielsen, M. M.; Jahn, K.; Subramani, R.; Mamdouh, W.; Golas, M. M.; Sander, B.; Stark, H.; Oliveira, C. L. P; *et al*. Self-Assembly of a Nanoscale DNA Box with a Controllable Lid. *Nature* **2009**, *459*, 73–76.
23. Schultz, S.; Smith, D. R.; Mock, J. J.; Schultz, D. A. Single-Target Molecule Detection with Nonbleaching Multicolor Optical Immunolabels. *Proc. Natl. Acad. Sci. U.S.A.* **2000**, *128*, 2115–2120.
24. O'Neal, D. P.; Hirsch, L. R.; Halas, N. J.; Payne, J. D.; West, J. L. Photo-thermal Tumor Ablation in Mice Using Near Infrared-Absorbing Nanoparticles. *Cancer Lett.* **2004**, *209*, 171–176.
25. Huang, X.; El-Sayed, I. H.; Qian, W.; El-Sayed, M. A. Cancer Cell Imaging and Photothermal Therapy in the Near-Infrared Region by Using Gold Nanorods. *J. Am. Chem. Soc.* **2006**, *128*, 2115–2120.
26. Aldaye, F. A.; Sleiman, H. F. Dynamic DNA Templates for Discrete Gold Nanoparticle Assemblies: Control of Geometry, Modularity, Write/Erase and Structural Switching. *J. Am. Chem. Soc.* **2007**, *129*, 4130–4131.
27. Sebba, D. S.; Mock, J. J.; Smith, D. R.; LaBean, T. H.; Lazarides, A. A. Reconfigurable Core-Satellite Nanoassemblies as Molecularly-Driven Plasmonic Switches. *Nano Lett.* **2008**, *8*, 1803–1808.
28. Wang, H.; Reinhard, B. M. Monitoring Simultaneous Distance and Orientation Changes in Discrete Dimers of DNA Linked Gold Nanoparticles. *J. Phys. Chem. C.* **2009**, *113*, 11215–11222.
29. Maye, M. M.; Kumara, M. T.; Nykypanchuk, D.; Sherman, W. B.; Gang, O. Switching Binary States of Nanoparticle Superlattices and Dimer Clusters by DNA Strands. *Nat. Nanotechnol.* **2010**, *5*, 116–120.
30. Zanchet, D.; Micheel, C. M.; Parak, W. J.; Gerion, D.; Alivisatos, A. P. Electrophoretic Isolation of Discrete Au Nanocrystal/DNA Conjugates. *Nano Lett.* **2001**, *1*, 32–35.
31. Deng, Z. X.; Tian, Y.; Lee, S. H.; Ribbe, A. E.; Mao, C. D. DNA-Encoded Self-Assembly of Gold Nanoparticles into One-Dimensional Arrays. *Angew. Chem., Int. Ed.* **2005**, *44*, 3582–3585.
32. Suzuki, K.; Hosokawa, K.; Maeda, M. Controlling the Number and Positions of Oligonucleotides on Gold Nanoparticle Surfaces. *J. Am. Chem. Soc.* **2009**, *131*, 7518–7519.
33. Mastroianni, A. J.; Claridge, S. A.; Alivisatos, A. P. Pyramidal and Chiral Groupings of Gold Nanocrystals Assembled Using DNA Scaffolds. *J. Am. Chem. Soc.* **2009**, *131*, 8455–8459.
34. Sharma, J.; Chhabra, R.; Cheng, A.; Brownell, J.; Liu, Y.; Yan, H. Control of Self-Assembly of DNA Tubules through Integration of Gold Nanoparticles. *Science* **2009**, *323*), 112–116.
35. Busson, M. P.; Rolly, B.; Stout, B.; Bonod, N.; Larquet, E.; Polman, A.; Bidault, S. Optical and Topological Characterization of Gold

Nanoparticle Dimers Linked by a Single DNA Double Strand. *Nano Lett.* **2011**, *11*, 5060–5065.
36. Bidault, S.; de Abajo, F. J. G.; Polman, A. Plasmon-Based Nanolenses Assembled on a Well-Defined DNA Template. *J. Am. Chem. Soc.* **2008**, *130*, 2750–2751.
37. Reinhard, B. M.; Sheikholeslami, S.; Mastroianni, A.; Alivisatos, A. P.; Liphardt, J. Use of Plasmon Coupling to Reveal the Dynamics of DNA Bending and Cleavage by Single EcoRV Restriction Enzymes. *Proc. Natl. Acad. Sci. U.S.A.* **2007**, *104*, 2667–2672.
38. Dubochet, J.; Lepault, J.; Freeman, R.; Berriman, J. A.; Homo, J. C. Electron-Microscopy of Frozen Water and Aqueous-Solutions. *J. Microsc.* **1982**, *128*, 219–237.
39. Dubochet, J.; Adrian, M.; Chang, J. J.; Homo, J. C.; Lepault, J.; Mcdowall, A. W.; Schultz, P. Cryo-Electron Microscopy of Vitrified Specimens. *Q. Rev. Biophys.* **1988**, *21*, 129–228.
40. Park, S.-J.; Lazarides, A. A.; Storhoff, J. J.; Pesce, L.; Mirkin, C. A. The Structural Characterization of Oligonucleotide-Modified Gold Nanoparticle Networks Formed by DNA Hybridization. *J. Phys. Chem. B* **2004**, *108*, 12375–12380.
41. Liu, J. W.; Lu, Y. Fast Colorimetric Sensing of Adenosine and Cocaine Based on a General Sensor Design Involving Aptamers and Nanoparticles. *Angew. Chem., Int. Ed.* **2006**, *45*, 90–94.